

End-to-End Multi-Task Deep Learning and Model Based Control Algorithm for Autonomous Driving

Der-Hau Lee^a, Jinn-Liang Liu^b

^aDepartment of Electrophysics, National Chiao Tung University, 1001 University Road, Hsinchu 300, Taiwan

^bInstitute of Computational and Modeling Science, National Tsing Hua University, 101, Section 2, Kuang-Fu Road, Hsinchu 300, Taiwan

Abstract

End-to-end driving with a deep learning neural network (DNN) has become a rapidly growing paradigm of autonomous driving in industry and academia. Yet safety measures and interpretability still pose challenges to this paradigm. We propose an end-to-end driving algorithm that integrates multi-task DNN, path prediction, and control models in a pipeline of data flow from sensory devices through these models to driving decisions. It provides quantitative measures to evaluate the holistic, dynamic, and real-time performance of end-to-end driving systems, and thus allows to quantify their safety and interpretability. The DNN is a modified UNet, a well known encoder-decoder neural network of semantic segmentation. It consists of one segmentation, one regression, and two classification tasks for lane segmentation, path prediction, and vehicle controls. We present three variants of the modified UNet architecture having different complexities, compare them on different tasks in four static measures for both single and multi-task (MT) architectures, and then identify the best one by two additional dynamic measures in real-time simulation. We also propose a learning- and model-based longitudinal controller using model predictive control method. With the Stanley lateral controller, our results show that MTUNet outperforms an earlier modified UNet in terms of curvature and lateral offset estimation on curvy roads at normal speed, which has been tested in a real car driving on real roads.

Keywords: Autonomous driving, multi-task deep learning, convolutional neural network, lane segmentation, path prediction, control algorithm.

1. Introduction

End-to-end driving system with a single deep neural network (DNN) is an emerging technology in autonomous vehicles [1, 2, 3, 4]. The system is a pipeline consisting of perception sensors, DNN, and control actuators [1, 2, 3] with a data flow from sensors to DNN to path planning to controllers to actuators for making driving decisions of steering, acceleration, or braking in an end-to-end, autonomous, and real-time manner [1, 2, 3, 5].

Since Pomerleau's pioneering work in the 1980s [6], a variety of end-to-end DNNs have been proposed for various tasks in autonomous driving [5, 7, 8, 9, 10, 11, 12, 13, 14, 15, 16, 17, 18, 19, 20, 21, 22, 23, 24]. Most of these DNNs belong to single-task learning models having single (regression or probabilistic) loss function for training the model to infer single driving task (steering angle, lead car's distance, or turning etc.) except those in [5, 15, 19, 20, 22].

Autonomous vehicles are equipped with various and numerous sensors (cameras, LiDARs, Radars, GPS etc.) to tackle complex driving problems (localization, object detection, scene semantics, path planning, maneuvers etc.) [25, 26]. Multi-task (MT) deep learning can usually achieve better performance than

its single-task (ST) counterparts due to more data from different tasks [27]. However, it remains a challenge to design MTDNNs that use fused multi-modal data to achieve stringent requirements of accuracy, robustness, and real-time performance in autonomous driving [25, 26].

There is another issue in end-to-end driving pipeline, namely, the integral system of DNN, path planning [4, 28, 29, 30, 31, 32], and control [5, 21, 33, 34, 35, 36, 37] algorithms that meets safety and comfort requirements. These algorithms are generally proposed and verified separately since automotive control systems are very complex varying with vehicle types and levels of automation [1, 38, 39, 40, 41, 42]. The literature is very scarce on the overall and dynamic evaluation of these algorithms in an integrated pipeline for multiple tasks using multi-modal data [5, 19, 20].

We propose here a multi-task deep learning model based on the well-known UNet architecture of image semantic segmentation [43, 44, 45, 46, 47, 48, 49, 50, 51, 52, 53, 54, 55, 56]. Our MTUNet can infer one segmentation, one regression, and two classification tasks for a vehicle to perform lane segmentation, estimate its heading angle, and classify its road path ahead and its distance to lead cars, respectively, using its multi-modal data of camera images, speed from control area network (CAN bus [57]), and radar signals of lead cars.

We also design an end-to-end driving algorithm that integrates all UNet, path prediction, and control models into a pipeline. The path prediction model comprises advanced post-

Email addresses: derhaulee@gmail.com (Der-Hau Lee),

jinnliu@mail.nd.nthu.edu.tw (Jinn-Liang Liu)

URL: <http://www.nhcue.edu.tw/~jinnliu> (Jinn-Liang Liu)

processing methods that are particularly suitable for deep learning to deal with complexity, scalability, and homography issues [8, 28, 58, 59, 60, 61]. The control model consists of learning-based lateral [5, 9, 10, 12, 14, 19, 21, 34, 37] and longitudinal [5, 19, 37] controllers, where the later is based on model predictive control [33, 37], i.e., it is a learning- and model-based controller [37].

1.1. Related work

End-to-end driving pipeline involves various components from many different fields as mentioned above. We restrict our discussions of related work to end-to-end models that integrate sensors, DNN, and controls in a pipeline.

Pomerleau [6] proposed a 3-layer fully-connected NN that takes images from a camera and a laser range finder as input and produces 46 output units to determine a driving direction for road following. LeCun et al. [7] used a 6-layer convolutional NN (CNN) that maps input images to steering angles for off-road obstacle avoidance.

Chen et al. [9] proposed a direct perception model that maps images to 14 affordance indicators using AlexNet [62] for fully autonomous driving on The Open Racing Car Simulator (TORCS) [63] which provides sophisticated sensory and graphical software engines to simulate corresponding electronic or mechanical devices in state-of-the-art vehicles [64].

Bojarski et al. [10] demonstrated that an end-to-end driving system with a CNN, which maps images directly to steering commands, can drive in traffic on roads with or without lane markings. The system was trained on the image and steering data from human driving, and was in autonomous mode about 98% of the time excluding lane changes and turns in on-road tests. A similar work by Chen and Huang [13] also shows that their CNN can directly map images to steering angles using the human driving data provided by comma.ai [65].

Sauer et al. [19] generalized the model in [9] to include high-level driving commands such as “turn left at the next intersection” based on another simulator Car Learning to Act (CARLA) [66]. They reduced 14 indicators to 6, namely, heading angle, distance to lead vehicle, distance to lane center, red light, speed sign, and hazard stop to deal with complex urban environments. They proposed a decoupled algorithm of proportional–integral–derivative (PID) longitudinal and Stanley lateral controllers. The maximum speed of ego car (Ego) in [19] is 20 km/h in single-lane traffic.

Cudrano et al. [21] proposed an end-to-end model that integrates sensors, a modified UNet, a path prediction (PP) algorithm using Ego’s heading angle θ and lateral distance Δ to lane center predicted from UNet, and controllers in a pipeline for center-line estimation but without showing the model architecture and its details. They tested the model in a real car driving on two different racetracks in curvedness without other cars and with a maximum speed of 54 km/h. Their results show important effects of UNet’s perception in motion on the PP algorithm that yields mean absolute errors up to 45.3 cm in the lateral displacement Δ .

1.2. Contribution

These works except [21] do not provide quantitative results showing the dynamic performance of the integrated algorithm of DNN, PP, and control models. Evaluation of dynamic performance is important since the algorithm implements the logic of autonomous vehicles in motion and in a holistic way [41]. It is also an important step towards safety measures and interpretability of end-to-end driving systems [1, 2, 3, 4]. We propose such an integrated algorithm consisting of a new UNet architecture for multi-task learning, a path prediction model [23] using UNet’s output, a modified lateral controller, and a model- and learning-based longitudinal controller.

We reduce 5 indicators in our previous work [5] to 2 (θ and Δ [21, 23]), change one overtaking classification in [5] to two pose classifications, and add a lane semantic segmentation [23] in the present work. The driving tasks are different between these two works. The coupled approach of lateral and longitudinal controllers in [5] aims at arbitrary lane changing and overtaking and thus requires to incorporate multiple sensors to avoid collisions in highway traffic [5]. We use here a decoupled approach with a modified lateral and a new longitudinal controller, which is mainly for lane keeping and car-following that constitute active driving assistance systems currently being developed and deployed to commercial vehicles for Level 2 autonomous driving [65].

2. Learning, planning, and control models

2.1. Multi-task UNets

Figure 1 illustrates the architecture of our MTDNN using UNets, ResUNet [49, 51] for example, as a backbone that can perform multiple (segmentation, regression, and classification) tasks for controllers to make steering, acceleration, and braking decisions. We refer to [23] for a brief survey of UNets related to autonomous driving and other applications.

Backbone and segmentation subnets. Backbone and segmentation subnets are encoder and decoder, respectively, and output lane segmentation masks. The UNet encoder consists several repeated blocks each of which has two convolution (conv) layers and one max pooling layer, where the corresponding channels and spatial dimensions are designed to be doubled and halved, respectively, from those of the previous block [43]. The decoder is symmetrical to the encoder in the numbers of blocks and layers and in the numbers of spatial and channel dimensions [43].

There are two kinds of skip connections in ResUNet as shown in Fig. 1. Each Up-Conv layer in a decoding block is concatenated (C) with the feature map of the corresponding encoding block of the same spatial and channel dimensions. The C-skip connection combines extracting and up-conv features for both global recognition and local detection, respectively [43]. Another connection is a short skip from the first to the third layer of every block including the middle block in Fig. 1, where the operation is addition (A-skip) to form residual functions so that the model is easier to optimize especially for

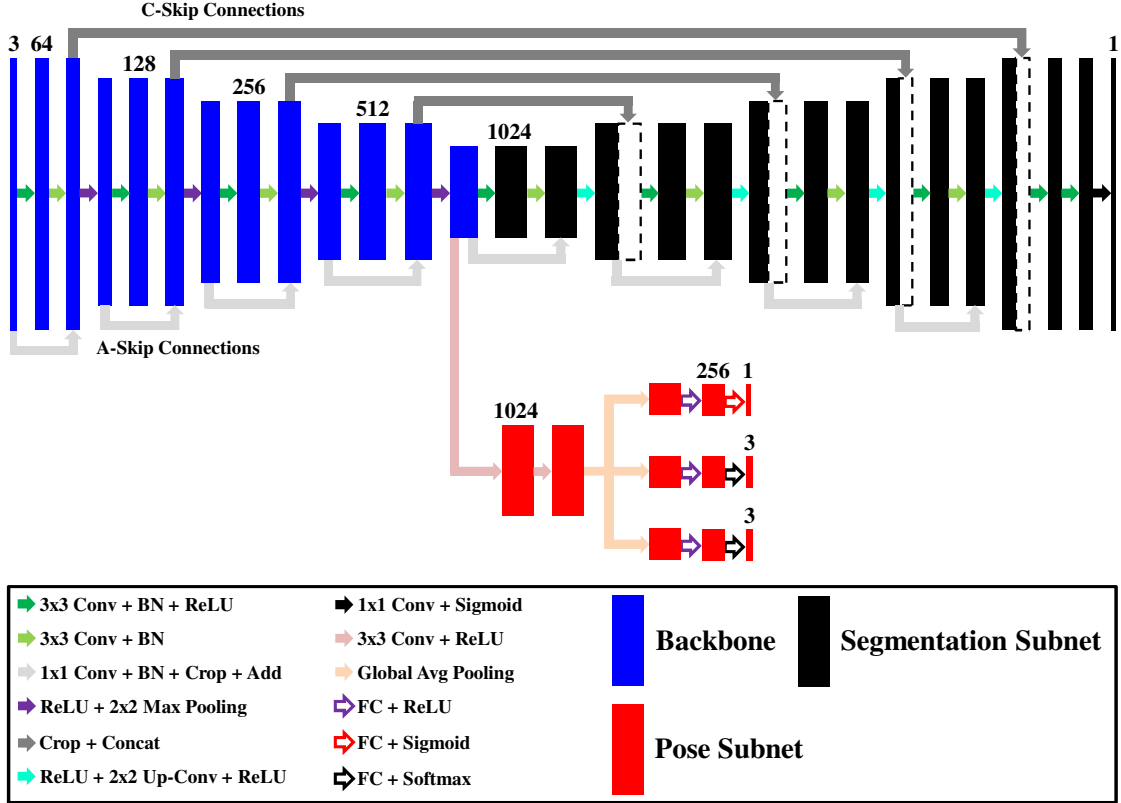


Figure 1: Multi-task UNet architecture with ResUNet for example. Each solid bar represents a feature map via the operations denoted by the arrow on its left side, where its channel number is on the top, except the first bar on the far left, which is an input image. The blue, black, and red bars correspond to backbone, segmentation, and pose subnets, respectively. Each dashed bar represents a concatenation (C) of a blue (extracting) map and a black (expanding) map of the same resolution by a C-skip connection shown as a long gray arrow. A in A-skip means addition. The outputs of MTUNets are lane gray image (GImg) from segmentation subnet and estimated Ego’s heading angle θ and probabilities of six classes (C1L, C1S, C1R, C2F, C2N, C2C, see text) of two classifications (C1, C2) from pose subnet, a total of four tasks, namely, one segmentation, one regression, and two classifications.

deep networks [67]. The output layers of the fourth and fifth blocks have a dropout rate of 50%.

The output of the segmentation subnet has the same resolution of the input image and a single channel from a pixel-wise sigmoid operation that yields a gray (probability) image (GImg) of lane lines [23] for the segmentation task. The normalized cross entropy loss [68]

$$L_S = - \frac{N}{P+N} \sum_{i=1}^P \log(\sigma(x_i)) \Big|_{\tilde{x}_i=1} - \frac{P}{P+N} \sum_{i=1}^N \log(1 - \sigma(x_i)) \Big|_{\tilde{x}_i=0} \quad (1)$$

is used to train MTResUNet with the other two tasks, where $x_i \in (0, 1)$ is a predicted score, $\tilde{x}_i = 0$ or 1 is the corresponding ground-truth value, P and N are the total numbers of positive (lane line) and negative (background) pixels in a batch of ground-truth images, respectively, and σ is the sigmoid function.

The segmentation subnet can thus generate a sequence of gray images of predicted lane lines with estimated lane width W and lateral offset Δ to lane centerline [23], which will be used in path prediction.

Pose subnet. This subnet connects to the last layer of the backbone and is designed to perform a regression task (the top branch of the subnet in Fig. 1) and a classification task (the other two branches) for Ego’s pose estimation and lead car (LCar) in the same lane, if any. The regression output estimates Ego’s heading angle while two classification outputs infer the road type (left turn, straight, or right turn) ahead Ego and LCar’s distance (far, nearby, or close) from Ego. These output classes will be defined more precisely later.

We have used two CNNs in [5] to estimate LCar’s distance by regression approach which yielded errors larger than 3 meters, far greater than that by radars (less than 10 cm [69]). However, radars cannot perceive obstacle categories like CNNs do with camera’s images. Therefore, we adopt classification approach here to perceive and categorize LCar into three classes in distance so that the classification output can be integrated with radar’s distance output into control algorithms [5] for autonomous driving.

The shared layers of the pose subnet consists of two convolutional layers and three parallel global average pooling (GAP) layers that extract features for the corresponding three branches of classification tasks at low spatial resolutions and are easier to interpret and less prone to overfitting [70]. Each branch has two fully connected (FC) layers followed by an activation (ReLU,

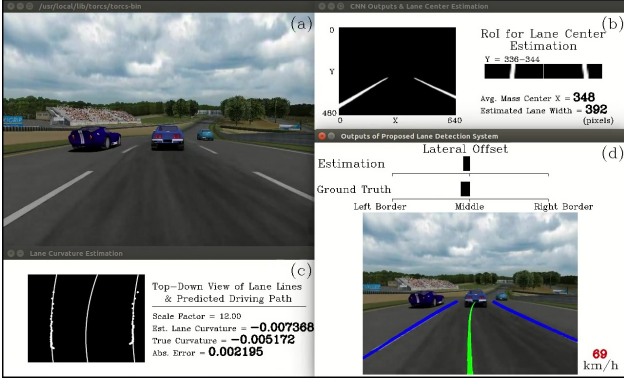


Figure 2: End-to-end driving model [23] consists of (a) input image, (b) lane detection by a modified UNet, (c) line clustering and perspective transformation, and (d) lateral offset estimation, inverse perspective transformation, line (blue) fitting, and driving path (green) prediction in TORCS traffic from Ego’s view without showing controllers.

sigmoid, or softmax) layer. Dropout applies to GAP and first FC layers to further prevent overfitting. The loss function of the regression task is a Euclidean L2 norm defined as

$$L_R = \frac{1}{2M} \sum_{i=1}^M |\tilde{\theta}_i - \theta_i|^2, \quad (2)$$

where $\tilde{\theta}$ and θ are normalized true and estimated values of Ego’s heading angle, respectively, and M is the batch size of input images. The cross-entropy

$$L_{C1,C2} = \frac{-1}{M} \sum_{i=1}^M \sum_{j=1}^3 \tilde{p}_{ij} \log(p_{ij}) \quad (3)$$

is for two classification tasks (C1 and C2), where \tilde{p} and p are true and sigmoid (C1) (or softmax (C2)) values of three classes, respectively. The three classes of C1 are denoted by C1L, C1S, and C1R for left turn, straight, and right turn, respectively, and C2F, C2N, and C2C of C2 for LCar’s far, nearby, and close distance.

The pose subnet does not change the topology of U-shaped network and can output multiple road predictions and pose estimations in a single forward pass, which are crucial in self-driving cars to make driving decisions [46]. Moreover, the combination of regression and classification losses yields a multi-modal loss that can avoid mode collapse problems when each individual task is trained alone [15, 25, 29, 32].

MTUNet and MTDSUNet have similar structures as shown in Fig. 1 except that MTUNet does not have skip connections, and MTDSUNet replaces the standard convolutions of MTResUNet by depthwise separable convolutions to improve computational complexity [23, 71]. Table 1 shows the complexity of these three models in the total number of parameters (Params), multiply-and-accumulates (MACs), and frames per second (FPS) in inference speed [72]. MTDSUNet is 2.26x lighter and 1.78x faster than MTResUNet in Params and FPS, respectively. We use MTUNets to denote the set of MTUNet, MTDSUNet, and MTResUNet. In all comparison tables, the best one appears in the last row.

Table 1: Complexity of MTUNets in parameters (Params), multiply-and-accumulates (MACs), and frames per second (FPS)

	Params	MACs	FPS
MTResUNet	47.38 M	70.37 B	23
MTUNet	45.99 M	67.46 B	26
MTDSUNet	20.96 M	14.50 B	41

2.2. Path prediction

In [23], we proposed an end-to-end learning model of single-task UNets with a PP algorithm that uses advanced methods to deal with complexity, scalability, and homography issues of CNN’s output images [58, 60, 61]. The model is generalized here to MTUNets, and summarized in Fig. 2 as a pipeline from input images (Fig. 2a) to driving decisions (Fig. 2d), where the output images are gray images (GImg) expressing the probability of each pixel in lane lines from 0 (black) to 1 (white) as shown in Fig. 2b, and control methods are extended to include both lane keeping and changing modes in Fig. 2d with more detail given below.

The PP algorithm takes a small region of interest (RoI in Fig. 2b) on each GImg, estimates a lateral offset Δ (Fig. 2d) to the ground-truth centerline of Ego’s lane in RoI, and then determines two parallel lane lines and their middle line (Fig. 2c) for Ego to travel. The parallel lines are obtained by quadratic polynomials that fit CNN’s semantic lines with recursive least squares [21] and imposing parallelism in the top-down view space from camera’s view via a perspective mapping [60, 61, 73]. Another quadratic polynomial for the desired driving path is then uniquely determined by three conditions, i.e., the starting (x_s) and final (x_f) points of the middle line of two parallel lines and its tangent at x_s as that of the parallel lines.

The tangent is replaced by Ego’s heading angle θ inferred by MTUNets in the present work. Therefore, θ and Δ are here outputs of MTUNets and PP, respectively, whereas tangent and Δ are both outputs of PP in [23]. Since MTUNets learn from road images to predict θ , it is important to feed annotated images to MTUNets with different classes like C1L, C1S, and C1R that teach MTUNets how to turn in lateral motion with meaningful θ , i.e., without mode collapsing.

For longitudinal motion, we design another three classes C2F, C2N, and C2C for MTUNets to learn how to roughly discern LCar’s distance in case that radar fails to detect LCar. Since TORCS is a perfect artificial simulator and never fails, the predicted values of these classes from the C2 branch are not used in our control algorithm below but only for investigating the C2 task in training phase.

2.3. Control

We use Ego’s heading angle θ and lateral offset Δ from MTUNets and PP to design a lateral controller. For longitudinal controller, we use Ego’s radar (Radar) data of LCar’s distance Δx and speed v_l and Ego’s CAN data of Ego’s speed v , where CAN is short for control area network, a standard network protocol [57] in modern vehicles. Car speed from CAN is

emulated in TORCS using gear change policy with revolutions per minute [74].

Using these data, we then propose an end-to-end learning based and model based [37] control algorithm that combines MTUNets, proportional and integral (PI) controller [37], Kalman filter (KF) [75, 76], and model predictive control (MPC) [37, 33] altogether to perform Ego’s lateral (steering) and longitudinal (acceleration or braking) maneuvers in a dynamic and real time traffic with other agent cars. The algorithm decouples lateral and longitudinal controllers and thus simplifies the complex control problem to a large extent [37] in contrast to coupled algorithms [5, 19].

Lateral controller. We define the steering command

$$\text{SteerCmd}(D, \theta, \Delta, v) = c_1 S_t \quad (4)$$

in discrete time t as a function of Ego’s driving desire D ($= 0$ for staying in current, -1 changing to left, or 1 to right lane), θ from MTUNets, Δ from PP, and Ego’s speed v by using the Stanley controller

$$S_t = \bar{S}_t - c_2(\bar{S}_t - S_{t-1}) \quad (5)$$

$$\bar{S}_t = \theta_t + \arctan\left(c_3 \frac{\Delta_t + DW}{v_t}\right), \quad (6)$$

which is a geometric trajectory tracking control model [19, 36, 37]. Here, c_1 is a constant normalizing the steering value to the range $[-1, 1]$, $c_2 = 0.5$ a damping parameter, $c_3 = 2.5$ a gain parameter, and $W = 4$ m a lane width (it can be a variable from CNN’s lane detection). The Stanley controller iteratively adjusts the steering angle to bring Ego to lane center.

Longitudinal controller. The discrete time PI controller [37]

$$\text{PI}(v) = u_t = k_p e_t + k_I \sum_{i=1}^n e_i \Delta\tau \quad (7)$$

is used to control Ego in longitudinal motion, where u_t is control action (acceleration) at current time t , $e_t = v_t - v_r$ is the error between Ego’s current (v_t) and reference (v_r) speed, n is the number of sampling instances, $\Delta\tau$ is the time between instances, and $k_p = 2$ and $k_I = 0.5$ are proportional and integral gains. The reference speed v_r is set to 76 km/h in cruise conditions for the most of our experiments and varies with Ego’s angle θ using tanh function in curvy conditions. The acceleration value is then normalized to

$$\text{AccelCmd}(u) = \tanh(u_t) \quad (8)$$

by the tanh function so is SteerCmd.

When a slower LCar is present, AccelCmd should be modified to maintain Ego’s safe distance to LCar, for which we use KF and MPC. The Kalman filter recursively predicts LCar’s current speed v_l and acceleration a_l from Radar’s past measurements $v_{l,k}$ of the speed for $k = 0, \dots, 99$ in a sampling period T_s [75, 76]. The model predictive control then predicts Ego’s acceleration a using KF’s v_l and a_l , LCar’s distance Δx_l from Radar, and Ego’s v_t from CAN.

We describe KF and MPC in detail as follows. LCar’s current state is denoted by the column vector $\mathbf{x} = [v_l a_l]^T$. The dynamic model

$$\mathbf{x}_k = \mathbf{A}\mathbf{x}_{k-1} \quad (9)$$

assumes a constant acceleration in T_s with the transition matrix

$$\mathbf{A} = \begin{bmatrix} 1 & T_s \\ 0 & 1 \end{bmatrix} \quad (10)$$

from $k-1$ to k and a null covariance matrix of process noises for simplicity. We use consecutive 100 data points ($k = 0, \dots, 99$) to predict LCar’s $v_{l,k}$ and $a_{l,k}$ with a ground true value of v_l being 18.33 m/s (66 km/h) and random numbers in the range of $[-3, 3]$ (m/s) to simulate noisy measurements. The measurements are scalars modeled as

$$z_k = \mathbf{H}\mathbf{x}_k + R, \quad (11)$$

where $\mathbf{H} = [1 \ 0]$ is a velocity measurement vector and $R = 5$ m/s a covariance of velocity measurement noises. A priori (with $-$ symbol) and a posteriori (without $-$) state estimates are then calculated by

$$\mathbf{x}_k^- = \mathbf{A}\mathbf{x}_{k-1}, \quad (12)$$

$$\mathbf{x}_k = \mathbf{x}_k^- + \mathbf{K}_k (z_k - \mathbf{H}\mathbf{x}_k^-), \quad (13)$$

$$\mathbf{K}_k = \mathbf{P}_k^- \mathbf{H}^T (\mathbf{H}\mathbf{P}_k^- \mathbf{H}^T + \mathbf{R})^{-1}, \quad (14)$$

$$\mathbf{P}_k^- = \mathbf{A}\mathbf{P}_{k-1}\mathbf{A}^T, \quad (15)$$

$$\mathbf{P}_k = (\mathbf{I} - \mathbf{K}_k \mathbf{H})\mathbf{P}_k^-, \quad (16)$$

where \mathbf{K}_k is Kalman gain and \mathbf{P}_k is covariance error with nonzero initial value \mathbf{P}_0 .

The inter-vehicle longitudinal dynamics model in [29, 77] denoted by $\text{MPC}(v, v_l, a_l, \Delta x_l)$ consists of

$$\Delta x_{k+1} = \Delta x_k + (v_l - v_k) T_s + \frac{1}{2} (a_l - a_k) T_s^2, \quad (17)$$

$$v_{k+1} = v_k + a_k T_s, \quad (18)$$

$$a_{k+1} = a_k + j_k T_s, \quad (19)$$

with $\Delta x_0 = \Delta x_t$, $v_0 = v_t$, $a_0 = 0$, and $j_0 = 0$ being Ego’s distance to LCar, speed, acceleration, and jerk, respectively, at current time t . The constraints of Ego’s variables are $5 \leq \Delta x_k \leq 15$ m, $0 < v_k \leq 30$ m/s, $-5 \leq a_k \leq 5$ m/s², and $-6 \leq j_k \leq 6$ m/s³ when following LCar.

Equations (17)-(19) and these constraints form an on-line optimization problem with the objectives

$$\max |\Delta x_k - D|, \min |a_k|, \text{ and } \min |j_k| \quad (20)$$

that yield safe, comfort, and fuel-economy car-following, respectively [29, 33], with a desired inter-distance D set to 15 m. The ACADO toolkit [77] is used to solve this problem with 50 control intervals in a total lapse of 50 s. The AccelCmd is then updated as

$$\text{AccelCmd}(u, a) = \frac{\tanh(u_t) + \tanh(a_1)}{2}. \quad (21)$$

The brake command

$$\text{BrakeCmd}(\Delta x) = \begin{cases} 0, & \Delta x_t \geq 7 \\ -\Delta x_t/2 + 3.5, & 5 < \Delta x_t < 7 \\ 1, & \Delta x_t \leq 5 \end{cases} \quad (22)$$

keeps Ego a safety distance of 5 m from LCar by gradually increasing its value from 0 to 1 with decreasing Δx_t when $5 \leq \Delta x_t \leq 7$ m.

We summarize all the above models, methods, and formulas into the following end-to-end algorithm implemented in this work from the input of road images from camera, Ego's speed v from CAN, and LCar's distance Δx and speed v_l from radar to the output values S , B , and A of three different actions from SteerCmd, BrakeCmd, and AccelCmd, respectively.

Learning and Model Based Control (LMBC) Algorithm

Input: CImg (road color image), v , Δx , v_l

Variables: C_d , θ , Δ , a , a_l , u

Functions:

UNet() returns lane GImg (gray) and Ego's heading angle θ

PP() returns Ego's lateral offset Δ in $[-2, 2]$

CAN() returns Ego's speed v

Radar() returns LCar's distance Δx and speed v_l

BrakeCmd() returns B in $[0, 1]$

SteerCmd() returns S in $[-1, 1]$

AccelCmd() returns A in $[-1, 1]$

PI() returns control u

KF() returns LCar's speed v_l and acceleration a_l

MPC() returns Ego's acceleration a in $[-5, 5]$

Control loop:

while (in self-driving)

GImg, θ = UNet(CImg); Δ = PP(GImg); v = CAN()

S = SteerCmd(D , θ , Δ , v)

u = PI(v)

Δx = Radar()

if (LCar exists)

B = BrakeCmd(Δx)

Δx , $v_{l,k=0-99}$ = Radar()

v_l , a_l = KF($v_{l,k=0-99}$) # Eqs. (12)-(16)

a = MPC(v , v_l , a_l , Δx) # Eqs. (17)-(19)

A = AccelCmd(u , a)

else

A = AccelCmd(u , $a = 0$)

Output: S , B , A

3. Experiment setup

This algorithm thus integrates deep learning, multi-task learning, multi-modal perception, and model-based control methods (LMBC) into an end-to-end mapping from a high dimensional space of image and car data to a three dimensional space of actions for autonomous driving. To assess its performance in static and dynamic conditions [5], we prepare and annotate input data for training and testing as follows.

Image data. We use the method in [5] to collect additional image data for this work with a modification. Ego drives normally with other agents on six different tracks [9] (not shown)

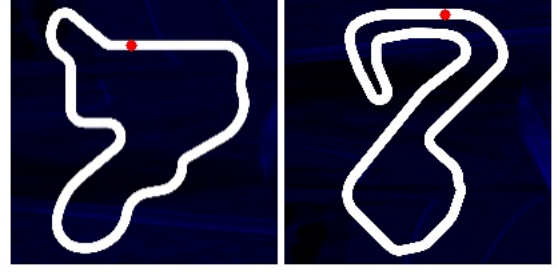


Figure 3: Tracks 7 (left) and 8 (right) for Ego and other agent cars all driving autonomously in test phase, where the lane width is 4 m, the total lengths are 2843 and 3919 m, respectively, the starting location is marked by a red symbol, and the driving direction is counterclockwise.

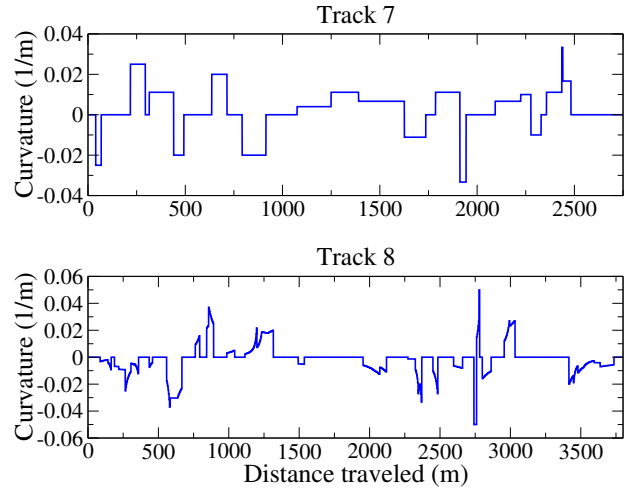


Figure 4: Curvature profiles of Tracks 7 and 8. Track 8 is curvier than Track 7, for example, the shape curves near 2800 m represent sudden changes in the road direction.

to collect 39,185 and 3,562 images for training and testing, respectively. It is normal instead of zigzag [5] driving because the number of affordance indicators reduces from five in [5] to only one here, and the LMBC algorithm is mainly for studying learning and model based controllers in lane keeping and car following maneuvers instead of autonomous lane changing and overtaking [5]. Another two tracks, namely, Tracks 7 and 8 in Fig. 3, are used to evaluate LMBC's dynamic performance in unseen environments. These two tracks are more curvy with curvature profiles shown in Fig. 4.

Labeling multi-modal data. Corresponding to each image, we use on-line CAN and radar ground-truth data of Ego's $\{\theta, v\}$ and LCar's $\{\Delta x, v_l\}$, respectively. Each image is labeled to one of three classes C1L, C1S, and C1R for road-type classification task according to its corresponding value of Ego's angle, where C1L, C1S, and C1R represent $\bar{\theta} < -0.006$ (left turn), $-0.006 \leq \bar{\theta} \leq 0.006$ (straight), and $0.006 < \bar{\theta}$ (right turn) in radian, respectively.

We annotate each image (the image resolution is 640×480) with bounding boxes to other cars and label the closest box as C2F, C2N, or C2C for boxA = 0 (far), $0 < \text{boxA} < 3200$

(nearby), or $3200 \leq \text{boxA}$ (close), where boxA denotes the area of the box in pixel^2 . The image is also processed to obtain a binary (black and white) image of lane-line masks as the ground-truth of lane segmentation for MTUNets. All binary images are similar to those annotated from real images [78]. Statistics of these labeled multi-modal data is summarized in Table 2.

Training strategy. MTUNets are trained in two stages. We first train the pose subnet by stochastic gradient descent with the batch size $\text{bs} = 20$, momentum $m = 0.9$, and learning rate starting from $\text{lr} = 0.01$ and decreasing by a factor of 0.9 every 5 epochs for a total of 100 epochs.

Segmentation and pose subnets are then trained jointly using the trained parameters of the model from the first stage and Adam optimizer with $\text{bs} = 1$, $m = 0.9$, and $\text{lr} = 10^{-4}$ and 10^{-5} for first 75 and last 25 epochs, respectively. Segmentation subnet is also trained independently with the same total number of parameters for a comparison between single and multi task cases. The total loss in each stage is a weighted sum of the corresponding losses in Eqs. (1) - (3).

Performance measures. Lane segmentation results from the segmentation subnet of MTUNets in Fig. 1 are expressed in pixel-wise true positive, true negative, false positive, and false negative values which are paired with ground truth values of lane lines in images. MTUNets' performance is measured in accuracy, precision, recall, and F1 score [8]. For the pose subnet, mean absolute error (MAE) and Accuracy are used to evaluate regression (Heading for θ) and classification (Road Type for C1 and LCar Dist. for C2) tasks, respectively.

4. Results and discussions

Table 3 shows that the performance of UNets is in the reverse order of their complexity in Table 1 as expected, i.e., the higher complexity of the model yields better measures but worse efficiency (FPS). Table 3 also shows that single-task (without MT) UNets outperform their multi-task (with MT) counterparts since the correlated tasks in the MT case obviously incur more errors than individual tasks. Nevertheless, differences between these two cases are very small in all measures. We exclude the worst DSUNet in Table 3 from what follows for further investigation on the dynamic performance of the LMBC algorithm when Ego drives along with other cars on Track 7/8 in Fig. 3.

The main objective of this work is to study the interplay among UNet, PP, PI, KF, and MPC models in the algorithm for Ego's lane keeping (lateral) and car following (longitudinal) maneuvers in autonomous driving with other cars. The algorithm accounts for Ego's variable speed (up to 76 km/h) and physical properties (weight 1150 kg, length 4.52 m, and width 1.94 m [63, 74]) to prevent sliding, slipping, and rollover in curves [79].

Table 4 and Fig. 5/6 show LMBC's dynamic performance using MTUNet and MTResUNet in real-time simulation at maximum speed 76/50 km/h on Track 7/8, where the dynamic mean absolute error (dMAE) [5] of predicted angle θ (blue curves in radian) and dMA lateral offset Δ (blue curves in m) are calculated while Ego is in motion. The ground-truth values (red

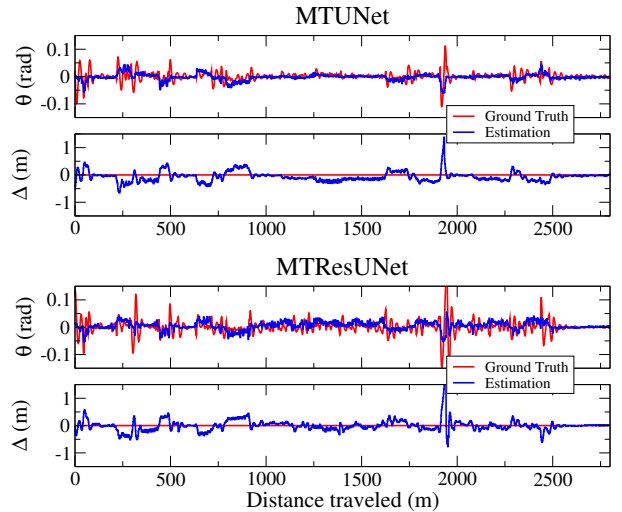


Figure 5: Dynamic performance of LMBC algorithm with MTUNets in θ -dMAE and dMA Δ for Ego's lane keeping maneuver along Track 7

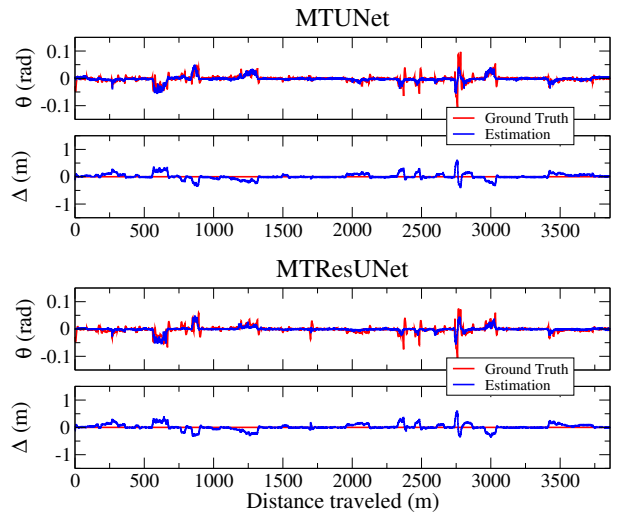


Figure 6: Dynamic performance of LMBC algorithm with MTUNets in θ -dMAE and dMA Δ for Ego's lane keeping maneuver along Track 8

curves) of θ and Δ are given by TORCS and set to zero, respectively.

The lateral indicators θ and Δ are crucial measures to quantify and interpret dynamic effects of CNN's perception on path planning in autonomous driving. LMBC with MTResUNet performs better than that of [21] (cf. Table 3), i.e., 0.0175/0.0059 vs. 0.029 and 12.8/6.5 vs. 45.3 cm in θ -dMAE and dMA Δ , respectively, in centered driving style on different (artificial vs. real-world) roads by different (artificial vs. real) cars at different maximum speeds (76/50 vs. 54 km/h). The end-to-end driving algorithm in [21] includes Δ calculations but without using learning methods for lateral corrections like our lateral offset estimation. The experimental roads in [21] are less curvy than Track 7/8. The minimum radius of general roads is about 130-160 m [80] corresponding to a maximum curvature of 0.00625-

Table 2: Statistics of labeled multi-modal data for multi-task UNets

Mode	CAN (θ, v)	Camera (image)			Radar ($\Delta x, v_l$)		
Task	Regression	Classification C1			Classification C2		
No. of frames	42747	Right turn	Straight	Left turn	Far	Nearby	Close
		8107	26179	8461	16405	11311	15031

Table 3: Performance of trained UNets for single (without MT) and multiple (MT) tasks on test data

	Segmentation Task				Pose Tasks		
	Accuracy	Precision	Recall	F1 Score	Heading MAE	Road Type Accuracy	LCar Dist. Accuracy
DSUNet	0.990	0.902	0.833	0.858	0.009	0.723	0.941
MT	0.988	0.837	0.831	0.828	0.007	0.681	0.942
UNet	0.995	0.933	0.911	0.921	0.004	0.970	0.952
MT	0.992	0.883	0.899	0.889	0.004	0.970	0.949
ResUNet	0.995	0.937	0.912	0.923	0.004	0.969	0.956
MT	0.993	0.898	0.893	0.893	0.004	0.968	0.954

Table 4: Performance of LMBC algorithm with MTUNets in the dynamic mean absolute error (dMAE) of Ego’s heading angle θ and dMA lateral offset Δ on Track 7/8 in Fig. 5/6

	Track 7		Track 8	
	θ (rad.)	Δ (m)	θ (rad.)	Δ (m)
MTUNet	0.0109	0.1418	0.0058	0.0633
MTResUNet	0.0175	0.1280	0.0059	0.0658

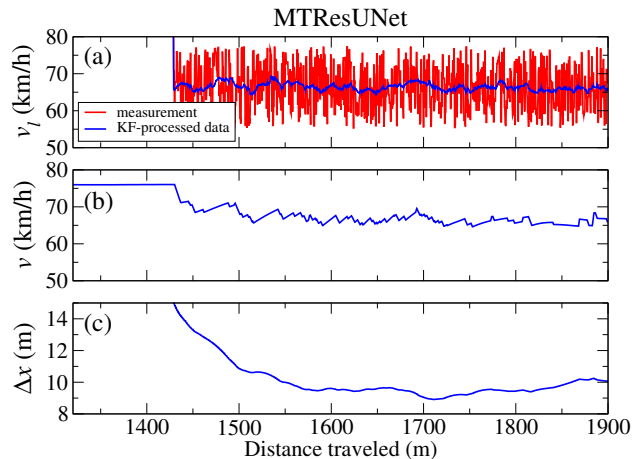
0.0076 whereas, for example, that of Track 7 is 0.05 m^{-1} . Table 4 and Fig. 5/6 thus postulate that LMBC may reduce dMA Δ to within 10 cm on real roads in future studies.

Li et al. investigated the lateral control of a MTCNN with 5 conv layers and a MT reinforcement learning (RL) model using TORCS and a multi-module method (perception and control modules) instead of end-to-end learning method [34]. They showed that MTRL outperforms MTCNN and yields 0.01 and 14.8 cm in θ -dMAE and dMA Δ , respectively, on a similar track. Our results are comparable to theirs as shown in Table 4.

Figure 7 presents longitudinal results of LMBC with MTResUNet in a nearly straight section of Track 8 when Ego cruises at 76 km/h and then follows LCar for 450 m. Here, v and v_l are Ego’s and LCar’s speed, respectively, Δx is their inter-distance, and v_l varies in the range of $[66-10.8, 66+10.8]$ km/h. LMBC effectively regulates v as shown in Fig. 7b according to v_l in Fig. 7a, and maintains Δx at about 10 meters in Fig. 7c. The iterative period of MPC and Kalman filter is about 35 and 0.15 (illustrated by red curves in Fig. 7a) ms, respectively.

Figures 5-7 thus show that the end-to-end LMBC algorithm effectively performs lateral and longitudinal maneuvers in terms of quantitative measures under dynamic, real-time, and variable driving conditions. We present a video on our website

for a qualitative review of LMBC’s performance in various lane keeping, car following, and lane changing scenarios in motion.

Figure 7: Longitudinal results of LMBC with MTResUNet on Ego’s car following for 450 m after traveling 1450 m, where v_l and v are LCar’s and Ego’s speed, respectively, and Δx is their distance.

5. Conclusion

We proposed an algorithm that combines multi-task UNet, path prediction, and control models, and uses camera images, radar signals, and car’s pose information as input data to perform end-to-end autonomous driving. We also proposed learning- and model-based controllers for lane keeping, car following, and lane changing maneuvers. Three UNet variants are firstly compared in complexity and four performance measures,

from which two are then compared in real-time simulation using dynamic measures of heading angle and lateral offset. Finally, the best one is chosen for further testing on car following. These measures are important to evaluate the safety and interpretability of end-to-end driving systems with single deep learning neural network. It is shown that our algorithm outperforms an earlier end-to-end model with another modified UNet, and is comparable to a reinforcement learning model, which is not end-to-end but multi-module.

References

- [1] S. Grigorescu, B. Trasnea, T. Cocias, and G. Macesanu, A survey of deep learning techniques for autonomous driving, *J. Field Robot.* 37 (3) (2020) 362-386.
- [2] A. Tampuu, T. Matiisen, M. Semikin, D. Fishman, and N. Muhammad, A survey of end-to-end driving: Architectures and training methods, *IEEE Trans Neural Netw Learn Syst.* (2020).
- [3] E. Yurtsever, J. Lambert, A. Carballo, and K. Takeda, A survey of autonomous driving: Common practices and emerging technologies, *IEEE Access* 8 (2020) 58443-58469.
- [4] C. Badue, R. Guidolini, R. V. Carneiro, P. Azevedo, V. B. Cardoso, A. Forechi, L. Jesus, R. Berriel, T. M. Paixão, F. Mutz, L. de P. Veronese, T. Oliveira-Santos, and A. F. De Souza, Self-driving cars: A survey, *Expert Syst. Appl.* 165 (2021) 113816.
- [5] D.-H. Lee, K.-L. Chen, K.-H. Liou, C.-L. Liu, and J.-L. Liu, Deep learning and control algorithms of direct perception for autonomous driving, *Appl. Intell.* 51 (2021) 237-247.
- [6] D. A. Pomerleau, *Alvin: An autonomous land vehicle in a neural network*, *Advances in neural information processing systems* (1989) 305-313.
- [7] Y. L. Cun, U. Muller, J. Ben, E. Cosatto, and B. Flepp, Off-road obstacle avoidance through end-to-end learning, *Advances in Neural Information Processing Systems* (2006) 739-746.
- [8] B. Huval, T. Wang, S. Tandon, J. Kiske, W. Song, J. Pazhayampallil, M. Andriluka, P. Rajpurkar, T. Migimatsu, R. Cheng-Yue, F. Mujica, A. Coates, and A. Y. Ng, An empirical evaluation of deep learning on highway driving, 2015, arXiv preprint arXiv:1504.01716.
- [9] C. Chen, A. Seff, A. Kornhauser, and J. Xiao, DeepDriving: Learning affordance for direct perception in autonomous driving, in: *Proceedings of the IEEE International Conference on Computer Vision*, 2015, pp. 2722-2730.
- [10] M. Bojarski, D. Del Testa, D. Dworakowski, B. Firner, B. Flepp, P. Goyal, L. D. Jackel, M. Monfort, U. Muller, J. Zhang, X. Zhang, J. Zhao, and K. Zieba, End to end learning for self-driving cars, 2016, arXiv preprint arXiv:1604.07316.
- [11] M. Al-Qizwini, I. Barjasteh, H. Al-Qassab, and H. Radha, Deep learning algorithm for autonomous driving using GoogLeNet, in: *IEEE Intelligent Vehicles Symposium (IV)*, 2017, pp. 89-96.
- [12] H. M. Eraqi, M. N. Moustafa, and J. Honer, End-to-end deep learning for steering autonomous vehicles considering temporal dependencies, 2017, arXiv preprint arXiv:1710.03804.
- [13] Z. Chen and X. Huang, End-to-end learning for lane keeping of self-driving cars, in: *IEEE Intelligent Vehicles Symposium (IV)*, 2017, pp. 1856-1860.
- [14] V. Rausch, A. Hansen, E. Solowjow, C. Liu, E. Kreuzer, and J. K. Hedrick, Learning a deep neural net policy for end-to-end control of autonomous vehicles, in: *American Control Conference (ACC)*, 2017, pp. 4914-4919.
- [15] H. Xu, Y. Gao, F. Yu, and T. Darrell, End-to-end learning of driving models from large-scale video datasets, in: *Proceedings of IEEE conference on computer vision and pattern recognition*, 2017, pp. 2174-2182.
- [16] M. G. Bechtel, E. McEllhiney, M. Kim, and H. Yun, DeepPicar: A low-cost deep neural network-based autonomous car, in: *IEEE Inter. Conf. on Embedded and Real-Time Computing Systems and Applications*, 2018, pp. 11-21.
- [17] F. Codevilla, M. Müller, A. López, V. Koltun, and A. Dosovitskiy, End-to-end driving via conditional imitation learning, in: *IEEE International Conference on Robotics and Automation*, 2018, pp. 1-9.
- [18] S. Hecker, D. Dai, and L. Van Gool, End-to-end learning of driving models with surround-view cameras and route planners, in: *Proceedings of the European Conference on Computer Vision*, Springer, 2018, pp. 435-453.
- [19] A. Sauer, N. Savinov, and A. Geiger, Conditional affordance learning for driving in urban environments, in: *Proceedings of the 2nd Conference on Robot Learning*, 2018, pp. 237-252.
- [20] M. Teichmann, M. Weber, M. Zoellner, R. Cipolla, and R. Urtasun, Multi-Net: Real-time joint semantic reasoning for autonomous driving, in: *IEEE Intelligent Vehicles Symposium (IV)*, 2018, pp. 1013-1020.
- [21] P. Cudrano, S. Mentasti, M. Matteucci, M. Bersani, S. Arrigoni, and F. Cheli, Advances in centerline estimation for autonomous lateral control, In: *IEEE Intelligent Vehicles Symposium (IV)*, 2020, pp. 1415-1422.
- [22] Y. Qian, J. M. Dolan, and M. Yang, DLT-Net: Joint detection of drivable areas, lane lines, and traffic objects, *IEEE Trans. Intell. Transp. Syst.* 21 (11) (2020) 4670-4679.
- [23] D.-H. Lee and J.-L. Liu, End-to-end deep learning of lane detection and path prediction for real-time autonomous driving, 2021, arXiv preprint arXiv:2102.04738.
- [24] W. Yuan, M. Yang, H. Li, C. Wang, and B. Wang, SteeringLoss: A Cost-sensitive loss function for the end-to-end steering estimation, *IEEE trans. Intell. Transp. Syst.* 22 (2) (2021) 1104-1113.
- [25] D. Feng, C. Haase-Schütz, L. Rosenbaum, H. Hertlein, C. Glaeser, F. Timm, W. Wiesbeck, and K. Dietmayer, Deep multi-modal object detection and semantic segmentation for autonomous driving: Datasets, methods, and challenges, *IEEE Trans. Intell. Transp. Syst.* 22 (3) (2020) 1341-1360.
- [26] S. Vandenhende, S. Georgoulis, W. Van Gansbeke, M. Proesmans, D. Dai, and L. Van Gool, Multi-task learning for dense prediction tasks: A survey, *IEEE PAMI*, (2021).
- [27] Y. Zhang and Q. Yang, A survey on multi-task learning, *IEEE Trans. Knowl. Data Eng.*, (2021).
- [28] C.-F. Lin, A. G. Ulsoy, and D. J. LeBlanc, Vehicle dynamics and external disturbance estimation for vehicle path prediction, *IEEE Trans. Control Syst. Technol.* 8 (3) (2000) 508-518.
- [29] M. Werling, J. Ziegler, S. Kammel, and S. Thrun, Optimal trajectory generation for dynamic street scenarios in a Frenét frame, in: *IEEE International Conference on Robotics and Automation*, 2010, pp. 987-993.
- [30] B. Paden, M. Čáp, S. Z. Yong, D. Yershov, and E. Frazzoli, A survey of motion planning and control techniques for self-driving urban vehicles, *IEEE Trans. Intell. Veh.* 1(1) (2016) 33-55.
- [31] W. Kim, C. M. Kang, Y. S. Son, S. Lee, and C. C. Chung, Vehicle path prediction using yaw acceleration for adaptive cruise control, *IEEE trans. Intell. Transp. Syst.* 19 (12) (2018) 3818-3829.
- [32] H. Cui, V. Radosavljevic, F.-C. Chou, T.-H. Lin, T. Nguyen, T.-K. Huang, J. Schneider, and N. Djuric, Multimodal trajectory predictions for autonomous driving using deep convolutional networks, in: *International Conference on Robotics and Automation (ICRA)*, 2019, pp. 2090-2096.
- [33] W. Qiu, Q. Ting, Y. Shuyou, G. Hongyan, and C. Hong, Autonomous vehicle longitudinal following control based on model predictive control, in: *2015 34th Chinese Control Conference (CCC)*, IEEE, 2015, pp. 8126-8131.
- [34] D. Li, D. Zhao, Q. Zhang, and Y. Chen, Reinforcement learning and deep learning based lateral control for autonomous driving, *IEEE Comput. Intell. Mag.* 14 (2) (2019) 83-98.
- [35] S. Dean, N. Matni, B. Recht, and V. Ye, Robust guarantees for perception-based control, 2019, arXiv preprint arXiv:1907.03680.
- [36] S. Thrun, M. Montemerlo, H. Dahlkamp, D. Stavens, A. Aron, J. Diebel, P. Fong, J. Gale, M. Halpenny, G. Hoffmann, K. Lau, C. Oakley, M. Palatucci, V. Pratt, P. Stang, S. Strohband, C. Dupont, L.-E. Jendrossek, C. Koelen, C. Markey, C. Rummel, J. v. Niekerk, E. Jensen, P. Alessandrini, G. Bradski, B. Davies, S. Ettinger, A. Kaehler, A. Nefian, and P. Mahoney, Stanley: The robot that won the darpa grand challenge, *J. Field Robot.* 23 (9) (2006) 661-692.
- [37] C. V. Samak, T. V. Samak, and S. Kandhasamy, Control Strategies for Autonomous Vehicles, 2021, arXiv preprint arXiv:2011.08729.
- [38] C. J. Taylor, J. Košecká, R. Blasi, and J. Malik, A comparative study of vision-based lateral control strategies for autonomous highway driving, *Int. J. Robot. Res.* 18 (5) (1999) 442-453.
- [39] A. Vahidi and A. Eskandarian, Research advances in intelligent collision avoidance and adaptive cruise control, *IEEE Trans. Intell. Transp. Syst.* 4 (3) (2003) 143-153.
- [40] S. A. Bagloee, M. Tavana, M. Asadi, and T. Oliver, Autonomous vehi-

- cles: Challenges, opportunities, and future implications for transportation policies, *Journal of Modern Transportation* 24 (2016) 284-303.
- [41] R. Hussain and S. Zeadally, Autonomous cars: Research results, issues, and future challenges, *IEEE Commun. Surv. Tutor.* 21 (2) (2019) 1275-1313.
- [42] J. Janai, F. Güneý, A. Behl, and A. Geiger, Computer vision for autonomous vehicles: Problems, datasets and state-of-the-art, 2021, arXiv preprint arXiv:1704.05519
- [43] O. Ronneberger, P. Fischer, and T. Brox, U-Net: Convolutional networks for biomedical image segmentation, in: *International Conference on Medical Image Computing and Computer-Assisted Intervention (MICCAI)*, Springer, 2015, pp. 234-241.
- [44] J. Long, E. Shelhamer, and T. Darrell, Fully convolutional networks for semantic segmentation, in: *Proceedings of the IEEE conference on computer vision and pattern recognition*, 2015, pp. 3431-3440.
- [45] Ö. Çiçek, A. Abdulkadir, S. S. Lienkamp, T. Brox, and O. Ronneberger, 3D U-Net: Learning dense volumetric segmentation from sparse annotation, in: *International Conference on Medical Image Computing and Computer-Assisted Intervention (MICCAI)*, Springer, 2016, pp. 424-432.
- [46] S. Mehta, E. Mercan, J. Bartlett, D. Weaver, J. Elmore, and L. Shapiro, Y-Net: Joint segmentation and classification for diagnosis of breast biopsy images, in: *International Conference on Medical Image Computing and Computer-Assisted Intervention (MICCAI)*, Springer, 2018, pp. 893-901.
- [47] T. Bruls, W. Maddern, A. A. Morye, and P. Newman, Mark yourself: Road marking segmentation via weakly-supervised annotations from multimodal data, in: *IEEE International Conference on Robotics and Automation (ICRA)*, 2018, pp. 1863-1870.
- [48] A. Rogriguez-Sanchez and A. Turečková, Isles challenge: U-shaped convolution neural network with dilated convolution for 3d stroke lesion segmentation, in: *International Conference on Medical Image Computing and Computer-Assisted Intervention (MICCAI)*, Springer, 2018, pp. 319-327.
- [49] X. Xiao, S. Lian, Z. Luo, and S. Li, Weighted Res-UNet for high-quality retina vessel segmentation, in: *9th International Conference on Information Technology in Medicine and Education (ITME)*, 2018, pp. 327-331.
- [50] X. Yang, H. Li, L. Wang, S. Y. Yeo, Y. Su, and Z. Zeng, Skin lesion analysis by multi-target deep neural networks, in: *Annual International Conference of the IEEE Engineering in Medicine and Biology Society (EMBC)*, 2018, pp. 327-331.
- [51] Z. Zhang, Q. Liu, and Y. Wang, Road Extraction by Deep Residual U-Net, *IEEE Trans. Geosci.* 15 (5) (2018) 749-753.
- [52] R. Li, M. Li, J. Li, and Y. Zhou, Connection sensitive attention U-NET for accurate retinal vessel segmentation, 2019, arXiv preprint arXiv:1903.05558.
- [53] N. Beheshti, and L. Johnsson, Squeeze U-Net: A memory and energy efficient image segmentation network, in: *IEEE/CVF Conference on Computer Vision and Pattern Recognition Workshops (CVPRW)*, 2020, pp. 1495-1504.
- [54] P. K. Gadosey, Y. Li, E. A. Agyekum, T. Zhang, Z. Liu, P. T. Yamak, and F. Essaf, SD-Unet: Stripping down U-Net for segmentation of biomedical images on platforms with low computational budgets, *Diagnostics* 10 (2) (2020) 110.
- [55] S. Guan, A. A. Khan, S. Sikdar, and P. V. Chitnis, Fully dense UNet for 2-D sparse photoacoustic tomography artifact removal, *IEEE J. Biomed.* 24 (2) (2020) 568-576.
- [56] L. Liu, J. Cheng, Q. Quan, and F.-X. Wu, A survey on U-shaped networks in medical image segmentations, *Neurocomputing* 409 (7) (2020) 244-258.
- [57] S. Corrigan, Introduction to the Controller Area Network (CAN), Texas Instruments, Application Report, 2002.
- [58] D. Neven, B. De Brabandere, S. Georgoulis, M. Proesmans, and L. V. Gool, Towards end-to-end lane detection: an instance segmentation approach, in: *IEEE Intelligent Vehicles Symposium (IV)*, 2018, pp. 286-291.
- [59] N. Garnett, R. Cohen, T. Pe'er, R. Lahav, and D. Levi, 3D-LaneNet: End-to-end 3D multiple lane detection, in: *Proceedings of the IEEE International Conference on Computer Vision*, 2019, pp. 2921-2930.
- [60] X. Li, J. Li, X. Hu, and J. Yang, Line-CNN: End-to-end traffic line detection with line proposal unit, *IEEE trans. Intell. Transp. Syst.* 21 (1) (2020) 248-258.
- [61] P. Lu, C. Cui, S. Xu, H. Peng, and F. Wang, SUPER: A novel lane detection system, *IEEE Trans. Intell. Veh.* 6 (3) (2021) 583-593.
- [62] A. Krizhevsky, I. Sutskever, and G. E. Hinton, ImageNet classification with deep convolutional neural networks, *Advances in Neural Information Processing Systems*, 2012, pp. 1097-1105.
- [63] B. Wymann, et al.: TORCS: The open racing car simulator, 2000.
- [64] F. Rosique, P. J. Navarro, C. Fernández, and A. Padilla, A systematic review of perception system and simulators for autonomous vehicles research, *Sensors* 19 (3) (2019) 648.
- [65] Active Driving Assistance Systems: Test Results and Design Recommendations, Consumer Reports, Nov. 2020, <https://data.consumerreports.org>, Accessed by Sept. 26, 2021.
- [66] A. Dosovitskiy, G. Ros, F. Codevilla, A. Lopez, and V. Koltun, CARLA: An open urban driving simulator, in: *Proceedings of the 1st Conference on Robot Learning*, 2017, pp. 1-16.
- [67] K. He, X. Zhang, S. Ren, and J. Sun, Deep residual learning for image recognition, in: *Proceedings of the IEEE conference on computer vision and pattern recognition*, 2016, pp. 70-778.
- [68] S. Xie and Z. Tu, Holistically-nested edge detection, in: *IEEE International Conference on Computer Vision (ICCV)*, 2015, pp. 1395-1403.
- [69] D. Göhring, M. Wang, M. Schnürmacher, and T. Ganjineh, Radar/lidar sensor fusion for car-following on highways, in: *The 5th International Conference on Automation, Robotics and Applications*, IEEE, 2011, pp. 407-412.
- [70] M. Lin, Q. Chen, and S. Yan, Network in network, arXiv:1312.4400, 2013.
- [71] F. Chollet, Xception: Deep learning with depthwise separable convolutions, in: *Proceedings of the IEEE conference on computer vision and pattern recognition*, 2017, pp. 1251-1258.
- [72] V. Sze, Y.-H. Chen, T.-J. Yang, and J. S. Emer, Efficient processing of deep neural networks: A tutorial and survey, *Proc. IEEE* 105 (12) (2017) 2295-2329.
- [73] S. Lee, J. Kim, J. S. Yoon, S. Shin, O. Bailo, N. Kim, T.-H. Lee, H. S. Hong, S.-H. Han, and I. S. Kweon, VPGNet: Vanishing point guided network for lane and road marking detection and recognition, in: *Proceedings of the IEEE International Conference on Computer Vision*, 2017, pp. 1947-1955.
- [74] J. Muñoz, G. Gutierrez, and A. Sanchis, A human-like TORCS controller for the simulated car racing championship, in: *Proceedings of the IEEE Conference on Computational Intelligence and Games*, 2010, pp. 473-480.
- [75] G. Welch and G. Bishop, An introduction to the Kalman filter, Univ. North Carolina, Chapel Hill, NC, USA, Lecture, 2001.
- [76] K. Saho, Kalman filter for moving object tracking: Performance analysis and filter design, *Kalman Filters - Theory for Advanced Applications*, IntechOpen, 2018, pp. 233-251.
- [77] B. Houska, H. J. Ferreau, and M. Diehl, ACADO toolkit-An open source framework for automatic control and dynamic optimization, *Optim. Control Appl. Methods.* 32 (3) (2011) 298-312.
- [78] Y. Ko, Y. Lee, S. Azam, F. Munir, M. Jeon, and W. Pedrycz, Key points estimation and point instance segmentation approach for lane detection, *IEEE Trans. Intell. Transp. Syst.* (2021).
- [79] M. Park, S. Lee, and W. Han, Development of steering control system for autonomous vehicle using geometry-based path tracking algorithm, *ETRI Journal* 37 (2015) 617-625.
- [80] K. Fitzpatrick, Horizontal Curve Design: An Exercise in Comfort and Appearance, *Transp. Res. Rec.* 1445 (1994) 47-53.